DOI: 10.61782/fa.2025.0465

FORUM ACUSTICUM
EURONOISE 2025

INCREASING THE SPATIAL ALIASING FREQUENCY OF CIRCULAR ARRAYS VIA BEAMFORMER ORDER REDUCTION

Filippo Maria Fazi and Nara Hahn
Institue of Sound and Vibration Research
University of Southapton, U.K.

ABSTRACT

Spatial aliasing may occur when the wavelength of a sound becomes smaller than twice the distance between neighbouring transducers, limiting the directivity of loudspeaker or microphone arrays at high frequencies. This paper focuses on uniform circular arrays and investigates how the spatial aliasing frequency can be increased by reducing the beamformer order. By leveraging the special structure of the circular harmonic orthogonality matrix, derived from Discrete Fourier Transform theory, it is shown that spatial aliasing of a given high-order harmonic impacts only one specific lower-order harmonic. Based on this property, a strategy is proposed to increase the spatial aliasing frequency by creating beamformers with an order smaller than the maximum possible for the given number of transducers. These theoretical findings are validated through simulations, demonstrating the trade-off between spatial aliasing frequency and beamformer directivity.

Keywords: *microphone arrays, loudspeaker arrays, spatial aliasing, 3D audio, sound field reproduction.*

1. INTRODUCTION

It is well known that loudspeaker and microphone arrays suffer from spatial aliasing at high frequencies, where the spacing between neighbouring transducers is more than half of the wavelength under consideration. In beamforming applications, spatial aliasing typically generates grating lobes in the directivity pattern of the array, whose magnitude and width are comparable to that of the main beam [1–3].

Various strategies have been proposed in an attempt to mitigate the effect of spatial aliasing [4–6].

In the specific case of circular or spherical arrays, the sound field is usually represented by means of a (generalised) Fourier series with circular or spherical harmonics and the array usually attempts to measure or reproduce the sound field up to a given Fourier order N, which depends on the number of transducers. When using this Fourier representation, the effect of spatial aliasing is that the estimation or reproduction of the sound field Fourier coefficients of order N or lower is degraded by the energy of higher order coefficients being folded back into the lower order.

In this work we exploit the special structure of spatial aliasing of uniform circular array, which is directly related to the DFT periodicity, to propose a strategy to mitigate the effect of spatial aliasing. More specifically, we exploit the fact that, given an array with maximum order N and assuming an odd number of loudspeakers L, the energy of the coefficients of order $N+1$ is folder to coefficient $-N$, that of coefficient $N+2$ is folder to coefficient $-(N-1)$ and so on. At low frequencies, the Fourier representation of the sound field is dominated by low orders. The energy of coefficients of higher order becomes progressively more significant with increasing frequency. The usual rule-of-thumb is that a coefficient is negligible if its order $|n| > kr$, where k is the wavenumber and r the radius of the array. Above a given frequency, the coefficients of the order $\pm(N+1)$, which cannot be captured or reproduced by the array, become relevant and, because of spatial aliasing, their energy is folded to the coefficient $\mp N$. The considerations above suggest that reducing the order of the array to $N-1$, that is deliberately removing the coefficients of order $\mp N$ from the sound field measured or reproduced by the array, will reject the spatial aliasing effect caused by coefficients $\pm(N+1)$. At an even higher frequency, the energy of orders $\pm(N+2)$ will become significant, but its aliasing effect can be rejected by reducing the array order to $N-2$, and so on. This array order reduction, however, causes a reduction of the array's spatial resolution, and a broadening of the main

lobe in beamforming applications.

Spatial aliasing reduction methods that rely on very similar reasoning were previously proposed in the literature, for example in [5].

The relevant theory of Fourier representation is reviewed in the next section, followed by theoretical results that are specific for microphone arrays and for loudspeaker arrays, in Section 3 and 4 respectively. The proposed strategy to mitigate spatial aliasing is presented in Section 5, and the results are validated by numerical simulations described in Section 6.

2. THEORY

For a given wave number k, the expression of single plane wave in 2D, with direction of arrival ϕ_T, unitary amplitude and zero phase at the origin is given by

$$p(r,\phi) = e^{jkr\cos(\phi-\phi_T)} \tag{1}$$

where (r,ϕ) are the polar coordinate of a point in $\mathbb{R}^2$. The assumed time dependency is $e^{j\omega t}$. Any sound field satisfying the homogeneous Helmholtz equation in $\mathbb{R}^2$ can be represented by the plane wave superposition

$$p(r,\phi) = \int_0^{2\pi} a(\theta) e^{jkr\cos(\phi-\theta)} d\theta \tag{2}$$

$$= 2\pi \sum_{n=-\infty}^{\infty} j^n J_n(kr) e^{jn\phi} A_n \tag{3}$$

where J_n are is the n-th order Bessel function. The last equality is due to the Jacobi-Anger expansion

$$e^{jkr\cos(\phi-\theta)} = \sum_{n=-\infty}^{\infty} j^n J_n(kr) e^{jn(\phi-\theta)} \tag{4}$$

$a(\theta)$ is the plane wave density (PWD) function, with Fourier coefficients A_n. For a single plane wave ϕ_T we have that $a(\theta) = \delta(\theta-\phi_T) = \sum_{n=-\infty}^{\infty} e^{jn(\theta-\phi_T)}/(2\pi)$ and, consequently, $A_n = e^{-jn\phi_T}/(2\pi)$.

This result can be extended to the case when an infinite rigid cylinder (perpendicular to the plane where the sound field is defined) is included. As shown, for example, in references [7] and [8] the formula of a sound field with PWD Fourier coefficients A_n at position (r,ϕ), either in free field or on the surface of an infinite rigid cylinder of radius r, is given by

$$p(r,\phi) = \sum_{n=-\infty}^{\infty} P_n e^{jn\phi} = 2\pi \sum_{n=-\infty}^{\infty} A_n b_n(kr) e^{jn\phi} \tag{5}$$

$b_n(kr)$ are the radial functions defined as [1]

$$b_n(kr) = \begin{cases} j^n J_n(kr) & \text{free-field} \\ \frac{-2j^{n+1}}{\pi kr H_n'(kr)} & \text{rigid cylinder} \end{cases} \tag{6}$$

j is the imaginary unity, $J_n(kr)$ is the n-th order Bessel function, and $H_n'(kr)$ is the derivative of the n-th order Hankel function of the second kind. Note that, because $j^{-n} = (-1)^n j^n$, $J_{-n} = (-1)^n J_n$, and $H_{-n}' = (-1)^n H_n'$, we have that $b_{-n} = b_n$.

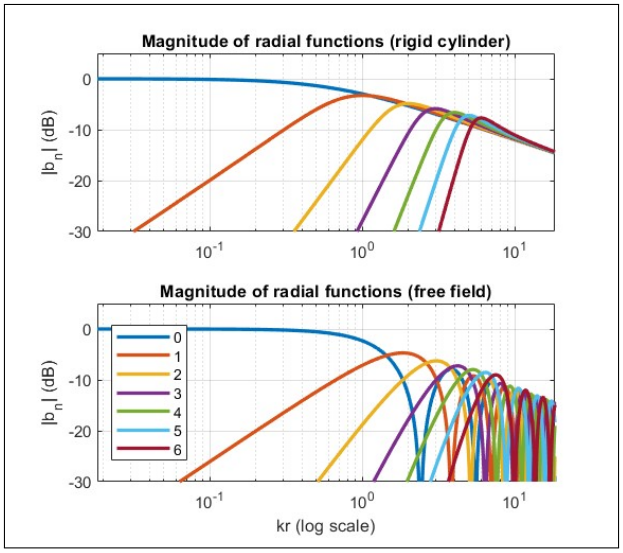

Figure 1. Magnitude of the radial functions b_n for different orders n, for the rigid cylinder case (top) and free-field case (bottom).

The radial functions are reported in Figure 1. It can be observed that high-order radial functions are negligible at low frequencies and their energetic contribution to the microphone signals becomes more significant with increasing frequency. This means that the radial functions act as high-pass filters for the Fourier coefficients A_n.

For both the case of the free field and the rigid cylinder, the magnitude of b_n increases monotonically in the low-frequency region, approximately where $kr < |n|$. This behaviour can be approximated with the small-argument approximation of Bessel and Hankel functions

[1] The definition of b_n has been adapted from [8], accounting for the different time convention used here ($e^{j\omega t}$).

[7], yielding

$$b_{|n|}(kr) \approx \frac{\epsilon_{|n|}}{|n|!}\left(j\frac{kr}{2}\right)^{|n|} \quad \text{for } kr \ll |n| \tag{7}$$

with

$$\epsilon_n = \begin{cases} 1 & \text{free-field} \\ 1 & \text{rigid cylinder with } n = 0 \\ 2 & \text{rigid cylinder with } n \neq 0 \end{cases} \tag{8}$$

It is interesting that the free-field and rigid-cylinder radial functions exhibit an almost identical low-frequency behaviour, with the difference that the rigid cylinder boosts all radial functions of order $|n| > 0$ by 6 dB.

As shown in the Appendix, the high-frequencies approximation of the radial functions is [7]

$$b_{|n|}(kr)| \approx \sqrt{\frac{2}{\pi kr}} d_{|n|}(kr) \text{ for } kr \gg |n| \tag{9}$$

$$d_{|n|}(kr) = \begin{cases} j^{|n|}\cos(kr - \pi/4 - |n|\pi/2) & \text{free-field,} \\ j^{|n|}e^{j(kr-\pi/4-|n|\pi/2)} & \text{rigid cylinder} \end{cases}$$

Note that the $|d_{|n|}| = 1$ for the rigid-cylinder case, and the radial function approximation decays monotonically and corresponds to the high-frequency approximation of $|H_0(kr)|$, for all orders n. Not surprisingly, this implies that all b_n have the same far-field decay as a line source. The cosine term in the free-field case represents the notches corresponding to the zeros of the Bessel functions, visible in Figure 1.

3. MICROPHONE ARRAYS

We consider now an array with L uniformly spaced microphones with angular coordinates $\phi_\ell = 2\pi\ell/L$, $\ell = 0, 1, \ldots L-1$. The Fourier coefficients P_n can be estimated with the discrete inverse Fourier series as

$$\tilde{P}_n = \frac{1}{L}\sum_{\ell=0}^{L-1} p_\ell e^{-jn\ell\frac{2\pi}{L}} \tag{10}$$

Substituting p_ℓ with equation (5) yields

$$\begin{aligned} \tilde{P}_n &= \sum_{m=-\infty}^{\infty} P_m \frac{1}{L}\sum_{\ell=0}^{L-1} e^{j(m-n)\ell\frac{2\pi}{L}} \\ &= \sum_{m=-\infty}^{\infty} P_m \sum_{z=-\infty}^{\infty} \delta_{n-m+zL} \\ &= \sum_{z=-\infty}^{\infty} P_{n+zL} \end{aligned} \tag{11}$$

where δ_n is the Kronecker delta. This central result, which is a direct consequence of the periodicity of the Fourier coefficients of discrete signals (or, equivalently, of the DFT), indicates that the estimation of the n-th order is contaminated by all coefficients with orders $n + zL$, for any integer number z. This is indeed the artefact caused by spatial aliasing .

The sound field coefficients A_n are estimated by inverting the radial functions b_n, namely

$$\tilde{A}_n = \frac{\tilde{P}_n}{2\pi b_n} = \sum_{z=-\infty}^{\infty} \frac{b_{n+zL}}{b_n} A_{n+zL} \tag{12}$$

Note that a regularisation scheme is usually applied to the inversion of the coefficients b_n to avoid instability, but this is not included here for the sake of simplicity [9].

Finally, the estimated plane wave density is

$$\begin{aligned} \tilde{a}(\theta) &= \sum_{n=-N}^{N} \tilde{A}_n e^{jn\theta} \\ &= \sum_{n=-N}^{N}\sum_{z=-\infty}^{\infty} \frac{b_{n+zL}}{b_n} A_{n+zL} e^{jn\theta} \end{aligned} \tag{13}$$

Note that the estimated PWD function $\tilde{a}(\theta)$ is, by construction, limited to order $N \leq (L-1)/2$, but the $2N+1$ coefficients $\tilde{A}_n$ will, in general, be different from the target coefficients A_n. Indeed, the two equations above clearly indicate that spatial aliasing causes the estimation of the coefficient A_n to be degraded by the energy shifting of the higher-order coefficients A_{n+zL}. This degradation, however, is mitigated by the ratio b_{n+zL}/b_n , whose magnitude is small at low frequencies. To show this, we observe that, in the frequency range where $kr \ll |n|, |n+zL|$, the radial function ratio can be approximated using eq. (7) as

$$\frac{b_{|n+zL|}}{b_{|n|}} \approx \frac{\epsilon_{|n+zL|}}{\epsilon_{|n|}} \frac{|n|!}{|n+zL|!}\left(j\frac{kr}{2}\right)^{|n+zL|-|n|} \tag{14}$$

This ratio has a frequency dependency of the form $\kappa_n(kr)^\alpha$. Assuming $|zL| > |n|$, the exponent $\alpha = |n+zL| - |n|$ is either $|zL|$ or $|zL| - 2|n|$, depending on the sign of $n \cdot z$. If we also assume that $L > 2|n|$, which is consistent with the usual requirement that $L \geq 2N+1$ [10], we have that $\alpha \geq 1$, and the radial function ratio above will decrease with decreasing frequency, with a slope of 20α dB/decade .

At high frequencies, the ratio $|b_{n+zL}|/|b_n|$ will tend to 1, as the magnitude of all radial functions has the same

asymptotic behaviour, as shown by eq. (9) (neglecting the notches due to the Bessel functions for the free-field radial functions).

4. LOUDSPEAKER ARRAYS

We want to synthesise a target, complex-valued directivity pattern $D(\theta)$ with a loudspeaker array consisting of infinite line sources arranged either on a circle or on the surface of an infinite cylinder.

Because of acoustical reciprocity, the far-field radiation pattern at a given direction θ due to a single infinite line source with unitary amplitude and located at point (r, ϕ), either in free-field or or on the surface of an infinite rigid cylinder, is the same as the sound field due to a plane wave from direction θ and measured by a microphone at (r, ϕ), given by equation (5) with $A_n = e^{-jn\theta}/(2\pi)$, namely

$$D(\theta - \phi) = \sum_{n=-\infty}^{\infty} b_n(kr) e^{jn(\theta-\phi)} \tag{15}$$

Considering now a continuos distribution of line sources on a circle with strength density function $q(\phi)$, the reproduced radiation patter is

$$\begin{aligned} D(\theta) &= \int_0^{2\pi} D(\theta-\phi) q(\phi) d\phi \\ &= \sum_{n=-\infty}^{\infty} b_n(kr) e^{jn\theta} \int_0^{2\pi} q(\phi) e^{-jn\phi} d\phi \\ &= 2\pi \sum_{n=-\infty}^{\infty} Q_n b_n(kr) e^{jn\theta} \end{aligned} \tag{16}$$

The coefficients Q_n that reconstruct a given target radiation pattern with Fourier coefficients D_n are therefore $Q_n = D_n/(2\pi b_n)$. A common choice in beamforming applications is the target directivity pattern $D(\theta) = \sum_{n=-N}^{N} e^{jn(\theta-\phi_T)}$, which is a a circular sinc function [10], also referred to as Dirichlet function. In this case, the coefficients $Q_n = e^{-jn\phi_T}/(2\pi b_n)$ for $|n| \leq N$ and 0 otherwise.

We now consider a uniform circular array of L sources at angular positions $\phi_\ell = \ell 2\pi/L$, $\ell = 0, 1, \ldots L-1$. The driving signals q_ℓ are given by the uniform spatial sampling of $q(\phi)$, namely

$$q_\ell = \frac{2\pi}{L} \int_0^{2\pi} \delta(\phi - \phi_\ell) q(\phi) d\phi \tag{17}$$

$$= \frac{1}{L} \sum_{n=-N}^{N} \frac{D_n}{b_n} e^{jn\ell\frac{2\pi}{L}} \tag{18}$$

The corresponding source strength density function is

$$\tilde{q}(\phi) = \frac{2\pi}{L} \sum_{\ell=0}^{L-1} q(\phi) \delta\left(\phi - \ell\frac{2\pi}{L}\right) \tag{19}$$

The Fourier coefficients of this train of delta functions is

$$\begin{aligned} \tilde{Q}_n &= \frac{1}{2\pi} \int_0^{2\pi} \tilde{q}(\phi) e^{-jn\phi} d\phi \\ &= \sum_{m=-\infty}^{\infty} Q_m \frac{1}{L} \sum_{\ell=0}^{L-1} e^{j(m-n)\ell\frac{2\pi}{L}} \\ &= \sum_{z=-\infty}^{\infty} Q_{n+zL} \end{aligned} \tag{20}$$

The mathematical manipulation used to obtain this result is analogous to that in the previous section. The Fourier coefficients of the reproduced directivity function are therefore

$$\begin{aligned} \tilde{D}_n &= 2\pi b_n \tilde{Q}_n = 2\pi b_n \sum_{z=-\infty}^{\infty} Q_{n+zL} \\ &= \sum_{z=-\infty}^{\infty} \frac{b_n}{b_{n+zL}} D_{n+zL} \end{aligned} \tag{21}$$

Note that this equation is similar to eq. (12) , but the roles of b_n and b_{n+zL} are swapped.

We assume in this work that the Fourier series of the target pattern is limited to order $N \leq (L-1)/2$ (i.e., $D_n = 0$ for $|n| > N$). With this assumption the equation above reduces to

$$\tilde{D}_n = \frac{b_n}{b_{\zeta(n)}} D_{\zeta(n)}, \text{ with } \zeta(n) = [(n+N) \mod L] - N$$

and the reproduced directivity pattern is

$$\tilde{D}(\theta) = \sum_{n=-\infty}^{\infty} D_{\zeta(n)} \frac{b_n}{b_{\zeta(n)}} e^{jn\theta} \tag{22}$$

An alternative formulation, based on eq. (21), is

$$\tilde{D}(\theta) = \sum_{m=-N}^{N} D_m \sum_{z=-\infty}^{\infty} \frac{b_{m+zL}}{b_m} e^{j(m+zL)\theta} \tag{23}$$

This result indicates that even if the target directivity $D(\theta)$ is limited to a given Fourier order N, the reproduced directivity function $\tilde{D}(\theta)$ will not be order-limited because of the occurrence of spatial aliasing. More specifically, the energy of each given order m of the target pattern is shifted to higher orders $m + zL$, with a modulation factor b_{m+zL}/b_m, which behaves similarly to a high-pass filter with a slope of $20\alpha = 20(|m + zL| - |m|)$ dB/decade, as shown above.

Note that the eq. (23) is similar but not identical to eq.(13). The main difference is that the estimated PWD $\tilde{A}(\theta)$ is order-limited, but its Fourier coefficients are corrupted by higher order. Conversely, the reproduced directivity pattern $\tilde{D}(\theta)$ is not order-limited, even if the target $D(\theta)$ is. The non-zero higher order coefficients D_{m+zL} are artefacts caused by spatial aliasing.

5. STRATEGY FOR SPATIAL ALIASING REDUCTION

We have established that the amount of spatial aliasing for a given order n is controlled by the ratio of radial functions b_{n+zL}/b_n . These radial function ratios are reported in Figure 2.

We observe that, as frequency increases, the order of the first unwanted coefficient $D_{n'}$ that will appear in the radiation pattern of a circular loudspeaker array as a consequence of the aliasing of D_n is $n' = -\text{sgn}(n)(L - |n|)$, with $|n'| > |n|$. Equivalently, for a microphone array the first sound field coefficient $A_{n'}$ with order $n' > N$ whose energy is folded into that of the measured coefficient A_n is, again, $n' = -\text{sgn}(n)(L - |n|)$.

In what follows the case of a loudspeaker array is analysed, but analogous considerations and results can be extended to microphone arrays.

The strategy proposed here is to attenuate the target coefficients $D_{|n|}$ above the frequency where the energy of the first aliased coefficient $D_{L-|n|}$ becomes significant. With increasing frequency, the highest order coefficeint D_N will be attenuated first, then the coefficient D_{N-1} and so on, down to a minimum order N_{min} below which a further order reduction is not desirable.

We will refer to these order-dependent low-pass filters as *anti-spatial aliasing (ASA) filters* , indicated by the symbol $F_n(kr)$. In practice, these filters will be integrated into the inverse radial filters $b_n^{(\text{inv})}$, namely

$$b_n^{(\text{inv})}(kr) = \frac{b_n(kr)^*}{|b_n(kr)|^2 + \beta} F_n(kr) \tag{24}$$

where we have now also applied Tikhonov regularisation with parameter β. The resulting source strength and reproduced beampattern will therefore be (see eq. (18) and (23))

$$q_\ell = \frac{1}{L} \sum_{n=-N}^{N} \frac{|b_n|^2}{|b_n|^2 + \beta} F_n \, D_n \, e^{jn\ell \frac{2\pi}{L}} \tag{25}$$

$$\tilde{D}(\theta) = \sum_{n=-N}^{N} D_n F_n \sum_{z=-\infty}^{\infty} \frac{b_{n+zL} b_n^*}{|b_n|^2 + \beta} e^{j(n+zL)\theta} \tag{26}$$

In the case of a beamformer, with $D_n = e^{-jn\phi_T}$, at frequencies where the coefficients are attenuated by the ASA filters the resulting beampattern will have a broader main lobe, but reduced grating lobes. Unfortunately, this aliasing reduction effect will appear only for a relatively restricted frequency range: it will no longer possible to mitigate the effect of spatial aliasing when the energy of the coefficient $\tilde{D}_{L-N_{min}}$ becomes significant, as this coefficient is not attenuated by the ASA filters. Note that $N_{min} > 0$, and setting $N_{min} = 1$ corresponds to requesting an omnidirectional target pattern when all ASA filters are active.

We shall now discuss the criteria for the ASA filter design. In this work, we design the ASA filters as zero-phase filters with the magnitude response of a Linkwitz-Riley highpass filter (consisting of two Butterworth filter is series), that is

$$F_n(kr) = \frac{1}{1 + \left(\frac{kr}{kr_n}\right)^{\mu_n}} \text{ for } n \geq N_{min} \tag{27}$$

$F_n(kr) = 1$ for $n < N_{min}$. Note that kr is used here as a single, dimensionless variable, as opposed to considering k and r separately. kr_n represents the cut-off frequency of the filters, and μ_n the filter order. The choice of zero-phase filters has the advantage of maintaining the phase-relation between coefficients of different orders, but with the significant practical disadvantage that the filters will be non-causal. Other filter type options are certainly possible, but this is left for future investigations.

The cut-off frequency kr_n can be defined by as the frequency where the radial function ratio has reached a desired threshold η:

$$kr_n = \arg\min_{kr} \left| \frac{|b_{L-|n|}|}{|b_{|n|}|} - \eta \right| \tag{28}$$

A closed form solution of the equation above can be found using the low-frequency approximation eq. (14) only

when $kr \ll |n|$, but this is generally true only for very small values of η. It may therefore be preferable to solve eq. (28) numerically.

The filter order μ_n may be chosen, for example, by imposing the filter slope to be the inverse of the slope of $b_{L-|n|}(kr)$ at low frequencies. Hence, in view of eq. (7) we define

$$\mu_n = L - |n| \tag{29}$$

Other options for μ_n are possible and their investigation is left for future work.

6. SIMULATIONS

The effectiveness of the proposed method has been validated with numerical simulations. To that end, the model of an ideal cylindrical loudspeaker array consisting of $L = 11$ line sources uniformly arranged on the surface of a rigid cylinder was created. The target directivity pattern was an $N = 5$ -order circular sinc function centred at $\phi_T = 0$:

$$D(\theta) = \sum_{n=-N}^{N} e^{jn\theta} \tag{30}$$

Its Fourier coefficients are therefore 1 for $n \leq N$ and 0 otherwise. Based on equation (18), the source driving functions were

$$q_\ell(kr) = \frac{1}{L} \sum_{n=-N}^{N} F_n(kr) \frac{b_n(kr)^*}{|b_n(kr)|^2 + \beta} e^{jn\phi_\ell} \tag{31}$$

with $\beta = 10^{-3.5}$.

The threshold value that defines the ASA filter cut-off frequencies, on the basis of eq. (28), was set to $\eta = 0.5$ (-6 dB). The lowest order to which the ASA filters were applied was $N_{min} = 3$. Figure 2 shows the magnitude of the radial function ratios $b_{L-|n|}/b_{|n|}$, for $0 \leq n \leq 5$. The plot confirms that these functions have a high-pass characteristic. The horizontal dashed red line is η (-6 dB), and the vertical black dashed line, corresponding to $|b_{L-|n|}|/|b_{|n|}| = \eta$, define the filter cut-off frequencies kr_n. The ASA filters are reported in Figure 3. Note that $|F_0| = |F_1| = |F_2| = 1$ because $N_{min} = 3$

Figure 4 depicts the inverse filters $b_n^{(\mathrm{inv})}(kr)$, as defined by eq. (24). The dashed lines are the magnitude of the inverse filters without ASA filter (i.e. $F_n = 1, \ \forall n$), whereas the continuous line are the inverse filters with ASA filters. The low frequency boost is due to the inversion of the low frequency roll-off of $b_n(kr)$, approximated

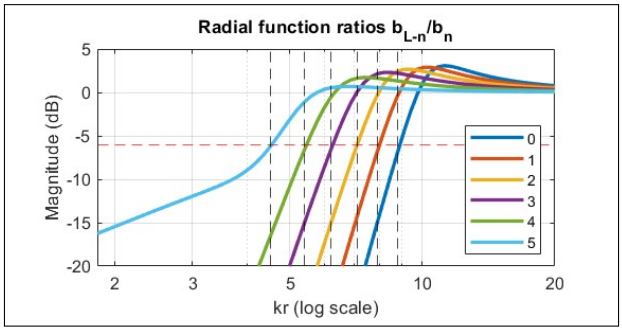

Figure 2. Radial filter ratios of for different orders n. The vertical dashed lines represent the filter cut-off frequencies kr_n. The horizontal dashed line is η.

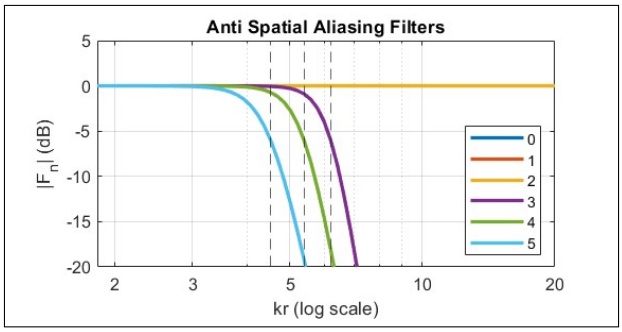

Figure 3. Magnitude of the ASA filters for different orders n. Note that $|F_0| = |F_1| = |F_2| = 0dB$. The vertical dashed lines represent the filter cut-off frequencies kr_n.

by eq. (7). The growth of $b_5^{(\mathrm{inv})}$ is limited to approximately 30 dB by the Tikhonov regularisation, whose effect is negligible at higher frequencies or for lower orders. The high frequency roll-off of $b_3^{(\mathrm{inv})}$,$b_4^{(\mathrm{inv})}$, and $b_5^{(\mathrm{inv})}$ is due to the ASA filters. Apart from this roll-off, the magnitude of all other inverse filters has the same asymptotic behaviour, corresponding to the inverse of eq. (9).

Figure 5 depicts the magnitude of the reproduced radiation pattern $\tilde{D}(kr, \theta)$, with and without ASA filters. The red vertical dashed corresponds to kr_6 , which is the frequency above which the energy of the first aliased coefficients b_6 becomes significant and it is provides an indication of the frequency above which spatial aliasing occurs if no ASA filter are applied. More rigorously, kr_6 is the frequency at which $|b_6(kr)|/|b_5(kr)| = \eta$. Recall that $N = (L-1)/2 = 5$ and $n = 6$ is the first order that cannot

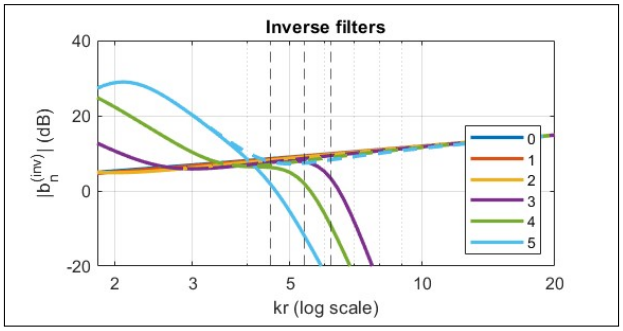

Figure 4. Magnitude of the inverse filters $b_n^{(\mathrm{inv})}(kr)$ for different orders n. The dashed lines correspond to the inverse filters without ASA filter, the continuous lines with the ASA filters. The vertical dashed lines represent the filter cut-off frequencies kr_n.

be controlled by the array. The green vertical corresponds to kr_9, which provides an indication of the frequency beyond which spatial aliasing occurs if the ASA filters are applied. This is because $n = 9 = L - (N_{min} - 1)$ is the first aliased order that is not attenuated by the ASA filters.

The two radiation patterns are almost identical for $kr < kr_6$. The expected effect of the ASA filters is clearly visible in the range $kr_6 < kr < kr_9$. The width of the main lobe progressively increases as a consequence of the order reduction caused by the ASA filters, and the grating lobes are significantly attenuated. This effect can be observed even more clearly in Figure 6, which reports the reproduced radiation pattern at $kr = 6$ (the black vertical dashed line in Figure 5), with and without ASA filters.

Above kr_9 the ASA filters are no longer effective. In fact, the reproduced pattern with ASA filters is not preferable to the pattern without those filters. This suggests that the proposed method provides an advantage only in the vicinity of the spatial aliasing frequency (corresponding to kr_6 in this example).

Finally, Figure 7 reports the Fourier coefficients $\tilde{D}_n(kr)$ of the reproduced pattern, for $0 \leq n \leq 11$, with (continuous lines) and without (dashed lines) ASA filters. It is clearly visible that beyond the cut-off frequencies kr_n of the ASA filters (black vertical dashed lines) the energy of the coefficients $\tilde{D}_5$, $\tilde{D}_4$ and then $\tilde{D}_3$ is attenuated, which is the causes of the broadening of the beamformer's main lobe observed in Figure 6. At the same time, the energy of the coefficients D_6, D_7 and D_8 is attenuated (see the difference between the continuous and dashed line),

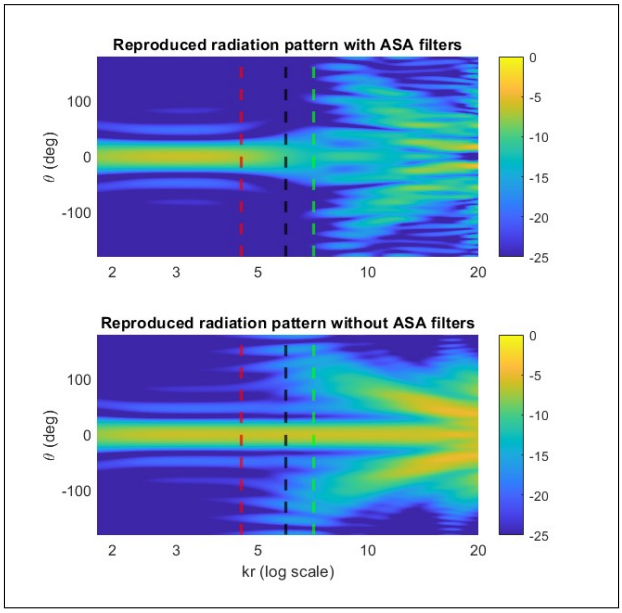

Figure 5. Reproduced radiation patter with (top plot) and without (bottom plot) ASA filters. The colour scale represents dB. The red and green dashed lines represent kr_6 and kr_9, respectively. The black dashed line corresponds to $kr = 6$, used in the single frequency plot in Figure 6.

thus mitigating the effect of spatial aliasing in this frequency range. The dashed vertical green line identifies kr_9, beyond which the energy of D_9 is greater than -6 dB and the effect of spatial aliasing becomes significant also when using the ASA filters. The low frequency roll-off of $\tilde{D}_5$ and $\tilde{D}_4$ (the latter is barely visible) is due to Tikhonov regularisation.

7. APPENDIX

High-frequency approximation of the radial functions, for $kr \gg n$. The derivation is based on results in reference [7]. For the rigid cylinder:

$$H_n'(x) = \frac{1}{2}(H_{n-1}(x) - H_{n+1}) \approx \sqrt{\frac{2}{\pi x}} j^{n-1} e^{-j(x-\pi/4)}$$

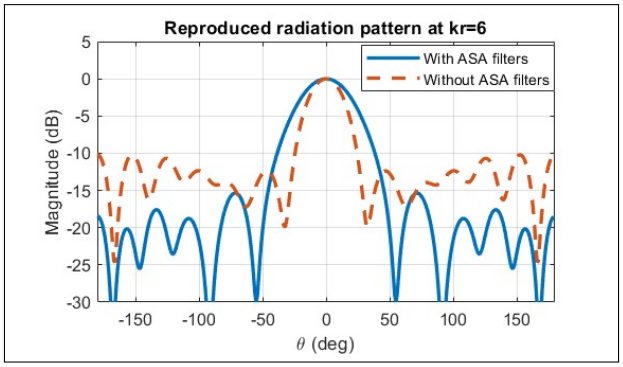

Figure 6. Normalised magnitude of the reproduced radiation pattern $\tilde{D}(\theta)$ for $kr = 6$. The dashed line corresponds to the inverse filters without ASA filters, the continuous lines with the ASA filters.

$$\begin{aligned} b_n(kr) &\approx \sqrt{\frac{\pi kr}{2}} \frac{-2j^{n+1}}{\pi kr j^{n-1} e^{-j(kr-\pi/4)}} \\ &= \sqrt{\frac{2}{\pi kr}} e^{j(kr-\pi/4)} [j^n e^{-n\pi/2}] \\ &= \sqrt{\frac{2}{\pi kr}} j^n e^{j(kr-\pi/4-n\pi/2)} \\ &\approx H_0(kr) \end{aligned}$$

For free field:

$$b_n(kr) = j^n J_n(kr) \approx j^n \sqrt{\frac{2}{\pi kr}} \cos(kr - n\pi/2 - \pi 4)$$

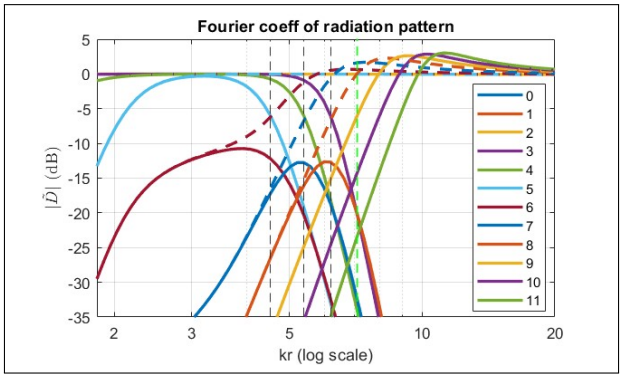

Figure 7. Magnitude of the Fourier coefficient $\tilde{D}_n$ of the reproduced radiation pattern, for different orders n. The dashed lines correspond to the coefficients without ASA filter, the continuous lines with the ASA filters. The vertical dashed lines represent the filter cut-off frequencies kr_n. The green dashed line is kr_9.

8. REFERENCES

[1] H. L. Van Trees, *Optimum array processing: Part IV of detection, estimation, and modulation theory*. John Wiley & Sons, 2002.

[2] J. Ahrens, *Analytic methods of sound field synthesis*. Springe, 2012.

[3] B. Rafaely, *Fundamentals of Spherical Array Processing*, vol. 8. Springer-Verlag Berlin Heidelberg, 1st ed., 2015.

[4] J. Meyer and G. W. Elko, "Handling spatial aliasing in spherical array applications," *Workshop on Hands-Free Speech Communication and Microphone Arrays*, pp. 1–4, 2008.

[5] A. Kuntz, *Wave Field Analysis Using Virtual Circular Microphone Arrays: Wellenfeldanalyse Mittels Virtueller Kreisförmiger Mikrofonanordnungen*. Verlag Dr. Hut, 2009.

[6] D. L. Alon and B. Rafaely, "Spherical microphone array with optimal aliasing cancellation," in *27th IEEE Convention of Electrical and Electronics Engineers in Israel*, pp. 1–5, 2012.

[7] E. G. Williams, *Fourier Acoustics. Sound Radiation and Nearfield Acoustical Holography*. London: Academic Press, 1st ed., 1999.

[8] H. Teutsch, *Modal Array Signal Processing: Principles and Applications of Acoustic Wavefield Decomposition*. Springer, 2007.

[9] F. Zotter, "A linear-phase filter-bank approach to process rigid spherical microphone array recordings," (Palić, Serbia), June 2018.

[10] M. A. Poletti, "A unified theory of horizontal holographic sound systems," *Journal of the Audio Engineering Society*, vol. 48, pp. 1151–1187, December 2000.